A COMBINED CLASSIFICATION SCHEME TO CHARACTERISE RIVER ICE FROM SAR DATA

Yves Gauthier[1], Frank Weber[2], Stéphane Savary[1], Martin Jasek[2], Lisa-Marie Paquet[1] and Monique Bernier[1]

1. INRS Eau, Terre et Environnement, Québec (Québec), Canada G1K 9A9; gautyves(at)ete.inrs.ca
2. BC Hydro, Burnaby (British Columbia), Canada V3N 4X8; frank.weber(at)bchydro.bc.ca

ABSTRACT

Rivers and streams are key elements in the terrestrial re-distribution of water. This is particularly so in winter, when the overland flow is minimal. An ice cover has a significant impact on rivers, as it affects the discharge capacity, can modify the ecosystem and microclimate, cause flooding, restrict navigation and impact hydropower generation. In the recent years, BC Hydro has been looking at the potential of RADARSAT-1 data (C-band, HH polarization) to classify river ice types and to determine ice cover characteristics for safe and efficient dam operations. The preliminary results of this project have confirmed that SAR data could provide valuable information about the ice front location and the ice conditions upstream and downstream of this point. This paper shows that a combination of texture and backscattering images improved the discrimination of ice cover types during freeze-up. RADARSAT-1 and ASAR data showed comparable backscattering profiles for 500 m averaged river reaches and produced comparable ice maps. However, in comparison with RADARSAT-1 fine beam images, the relatively coarse resolution of the ASAR data further reduces the sensitivity of the classification by missing details and incorrectly classifying mixed pixels. The addition of the vertical polarization did not add significant skill to the classification.

Keywords: River ice, SAR data, texture, unsupervised classification.

INTRODUCTION

Rivers and streams are key elements in the terrestrial re-distribution of water. This is particularly so in winter, when the overland flow is minimal. An ice cover has a significant impact on rivers, as it affects the discharge capacity, can modify the ecosystem and microclimate, cause flooding, restrict navigation and impact hydropower generation. Canada is renowned for its magnificent rivers, its harsh but beautiful winters and its large hydroelectric industry. The impact of the winter regime of Canadian rivers on the operation of hydroelectric facilities justifies extensive monitoring of the river ice cover.

For example, river ice processes on the Peace River are of great importance to the British Columbia Hydro and Power Authority (BC Hydro). The Peace River originates to the west of the Rocky Mountains in the Province of British Columbia (Canada). It flows in a northeasterly direction across the Province of Alberta before emptying into the Slave River. Located at its headwaters is the W.A.C. Bennett dam which forms Williston Reservoir. The flow regulation resulting from construction of the dam has altered the downstream flows. To meet the high energy demand during the winter months, winter flows have significantly increased, while the spring freshet has been attenuated. Monitoring the ice front location and ice cover characteristics during the winter is essential to conduct efficient dam operations and prevent undesired high water levels in the river or prevent potential ice jam related flooding downstream of the dam. Aerial surveys and field trips in such a remote and large area are costly and provide localised information only. By comparison, SAR remote sensing could be a reliable alternative owing to the advantages of spatial coverage, fine resolution and all weather capability. Furthermore, the signal emitted from a SAR sensor at 5.3 GHz is

able to penetrate the overlying dry snow cover and can provide information on the characteristics of the ice cover below.

Although some preliminary studies describe the interaction of radar and fresh water ice (1,2,3,4), it is still uncertain, which characteristics of the river ice cover really control the backscattering signal. The most accepted hypothesis is that the roughness at the ice-water interface is the dominant factor. It is assumed that the electromagnetic wave penetrates the ice cover due to a low dielectric contrast at the air-ice interface. At the ice-water interface, the dielectric contrast (ratio) is large and the signal is mostly reflected. When micro-roughness at the ice bottom is at least comparable to wavelength (5 cm), it starts to create scattering in different directions and therefore increases image backscattering. This backscatter would even be stronger if the bottom surface of the ice was perpendicular to the incoming radar beam. The ice structure within the ice cover also needs to be taken into consideration because inclusions in the ice, such as columnar or spherical air bubbles can cause volume scattering. Volume scattering may eventually prove helpful to discriminate between black ice (no inclusion) and white ice (snow ice, frazil ice). In shallow waters, the freezing of water to the channel bed creates a low dielectric contrast at the ice-riverbed interface, thereby causing a relatively weak backscattering. In the presence of calm open water, the dielectric contrast at the air-water interface is large and the resultant surface scattering component is reflected away from the radar, causing minimal backscatter on the image. If wind or rapids cause the micro-roughness of the water surface to be at least comparable to the wavelength, the signal is scattered in different directions, which in turn, causes a relatively strong backscattering. In this case, it is harder to discriminate between open water and the ice cover.

In the recent years, BC Hydro has been looking at the potential of RADARSAT-1 data (C-band, HH polarization) to classify river ice types and to determine ice cover characteristics (5,6) on the Peace River (Alberta, Canada). Promising results were obtained from a semi-automated river ice classification. Ice types and their spatial distribution along the river were determined with reasonable accuracy from RADARSAT-1 data. Furthermore, a correlation between the backscattering signal and the total ice thickness was found. Research efforts on the use of SAR data for monitoring the Peace River ice cover have been extended throughout 2004 and this paper summarizes the results from an analysis of the latest backscattering profiles along the river and the improvements to the classification scheme. In addition, ENVISAT-ASAR data were analyzed in an attempt to increase temporal SAR coverage over the area of interest.

The test area is a 60km long river reach upstream of the town of Peace River (Alberta) (Figure 1). At that point, the Peace River has a mean annual discharge of 1,830 m³/s, a drainage area of 186,000 km² and a channel width of about 300 m. The river channel is embedded in the lacustrine sediments/tills of the Peace River Lowlands.

METHODS

To achieve the objectives of the project, four RADARSAT-1 fine mode images (HH polarization, 8m spatial resolution, 1 look) and three ENVISAT-ASAR Standard mode images (HH-VV polarization, 25 m spatial resolution, 2 looks) were acquired over the study area in January and February of 2004.

Table 1: Acquired SAR images

RADARSAT-1 images (C-band)		ASAR images (C-band)	
Date	**Beam (incidence angles)**	**Date**	**Beam (incidence angles)**
10 January 2004	F4 (43.5°-45.8°)	01 February 2004	IS6 (39.1°-42.8°)
20 January 2004	F1N (36.4°-39.5°)	10 February 2004	IS2 (19.2°-26.7°)
27 January 2004	F2F (39.5°-42.5°)	20 February 2004	IS5 (35.8°-39.4°)
20 February 2004	F2F (39.5°-42.5°)		

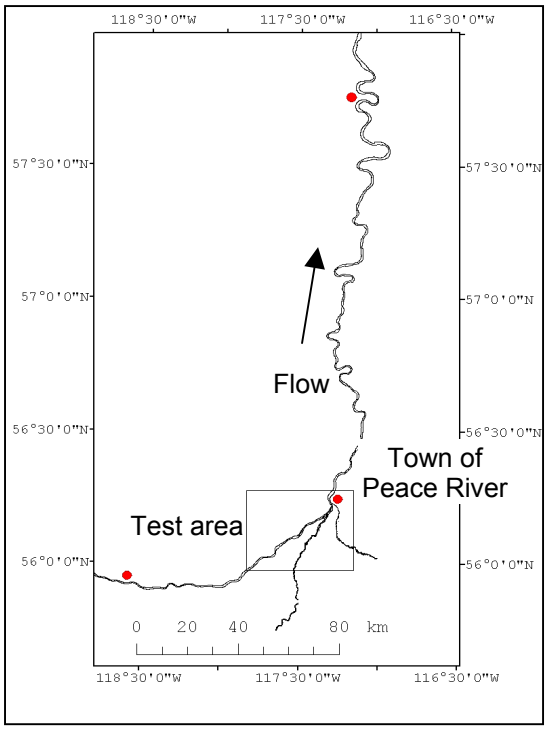

Figure 1: Location of test area.

Three corner reflectors were constructed and installed along the river to provide accurate control points for orthorectification of all images. Field measurements were conducted simultaneously with image acquisition. Four cross sections were surveyed on each visit. Cross section data consisted typically of 15 samples of snow depth, thermal thickness, total thickness, water level, and 'sail height'. These parameters are defined as follows: on rivers, thermal ice forms between frazil ice pans and in calm secondary channels due to the radiative cooling of water. Total ice thickness includes the thickness of thermal ice, which forms on the water surface, the thickness of juxtaposed or consolidated pans, which project down into the water, and frazil slush, which may accumulate below. Thermal ice thickness was measured through bore holes with a measuring stick which was hooked under the thermal ice cover. Total ice thickness was measured through bore holes using a submersible video camera which was mounted on an extendable (up to 11 m long) measuring rod. 'Sail height' is a measure of the surface roughness of the ice cover. It is measured from the thermal ice surface up to the average top of larger protruding pieces of ice by visually lining them up with the horizon.

On February 20, an aerial survey was conducted to determine spatial distribution of surface cover types. From a recent Landsat-7 ETM+ panchromatic image (15m spatial resolution), the river channel, islands and sand bars were manually digitized to create a mask of the river. Under this mask, the river was evenly divided into 500m long sections. These sections were edited to cover the main channel only and remove open water leads (Figure 2). The radar backscattering coefficients were then averaged over these sections to provide a backscattering profile of the ice cover at a 500 m resolution.

The original backscattering images were prepared for classification using two processing methods. Firstly, images were processed according to a filtering approach, as previously used by (5). The original 16 bit power images were scaled to 8 bit in order to reduce data size and increase processing speed. A Kuan filter was applied to reduce speckle. The resulting images were then filtered again with a median filter to achieve further smoothing. The second approach uses the original 16 bit power image to create a texture image. A texture image extracts information from the spatial distribution pattern of the backscatter values. As comprehensively explained in (7), the texture parameters are based on the grey level co-occurrence matrix (GLCM), which is a tabulation of how often different combinations of pixel brightness values (grey levels) occur in an image.

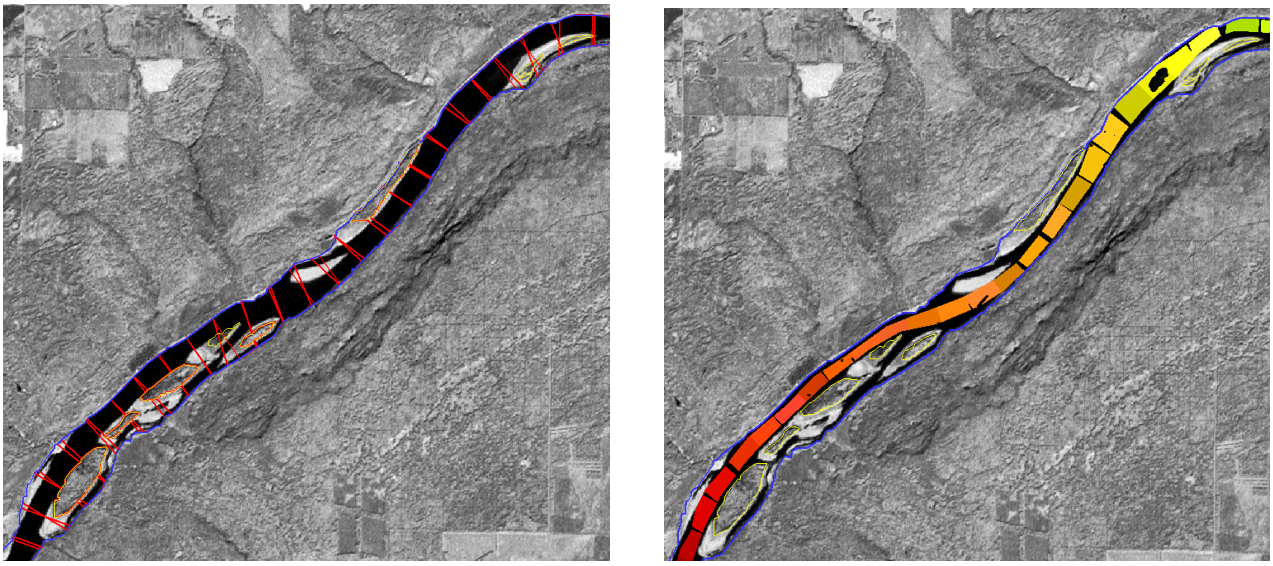

Figure 2: Generating channel sections (500 m spacing)

The GLCM is a normalized value, which is expressed as a close approximation of a probability table, $P(i,j)$, using:

$$P(i,j) = V(i,j) \Big/ \sum_{i,j=0}^{N-1} V(i,j) \tag{1}$$

where $V(i,j)$ is the grey level value of a cell with the coordinates *i* and *j*. The range of summation, $i,j = 0$ to $N-1$ means that each cell in the GLCM should be considered.

GLCM contrast, GLCM entropy, GLCM correlation, and GLCM mean texture images were considered in this study. Since this study showed it to reduce speckle most effectively, the GLCM mean texture image was considered to be the most suitable for a pixel-based classification. GLCM mean texture differs from a standard average filter, because the pixel value is weighted by its frequency of occurrence in combination with a certain neighbour pixel value and not by its frequency of occurrence by itself (7), based on the following equation:

$$\langle i \rangle = \sum_{i,j=0}^{N-1} i \cdot P(i,j) \tag{2}$$

A 7×7 window was selected for RADARSAT-1 images, in order to take into account the high image resolution of 8 m and the large river channel width of about 300 m. For the lower resolution ASAR data (25 m), a smaller 5×5 window was used. It should be noted that the texture approach is a relative approach, as it scales each image from 0 to 255, regardless of the underlying histogram and contextual pattern of each image. However, the texture is calculated over the entire image, thereby covering a wide range of patterns. We, therefore, assume that the texture values observed over the river on different dates are comparable.

Efficiency of both methods as input to ice type classification is assessed through the fuzzy *k*-Mean unsupervised algorithm, which segments the image according to an iterative measurement of the distance to class mean and a predetermined number of desired clusters. Data are bound to each cluster by means of a Membership Function, which represents the fuzzy behaviour of this algorithm. A complete description of the algorithm can be found in (8). The maximum number of classes was initially set to seven, which was found to be the number of ice cover types discernable by eye during freeze-up (5). The resulting classifications are compared to on-the-ground and aerial field observations.

RESULTS

Backscatter analysis

Figure 3 shows the backscattering profile averaged over 500 m sections along the main channel for four RADARSAT-1 images. On January 10, an aerial survey located the ice front near km 391.5 at midday. We estimate the location at the time of image acquisition (7:00 am) to be around km 394. Upstream of the ice front, frazil pan concentrations ranging from low to high and open water were observed. On the backscatter profile the increasing concentration of frazil pans towards the head of the complete ice cover causes the rapid increase of the backscatter. The first peaks at -4.8 dB and -4.3 dB (around km 395) actually correspond to the first 500 m averaging sections without open water leads. Downstream from this point, the ice cover ranged from juxtaposed to consolidated, with occasional open water leads, which cause averaged backscatter values to range from -6.5 to -1.6 dB.

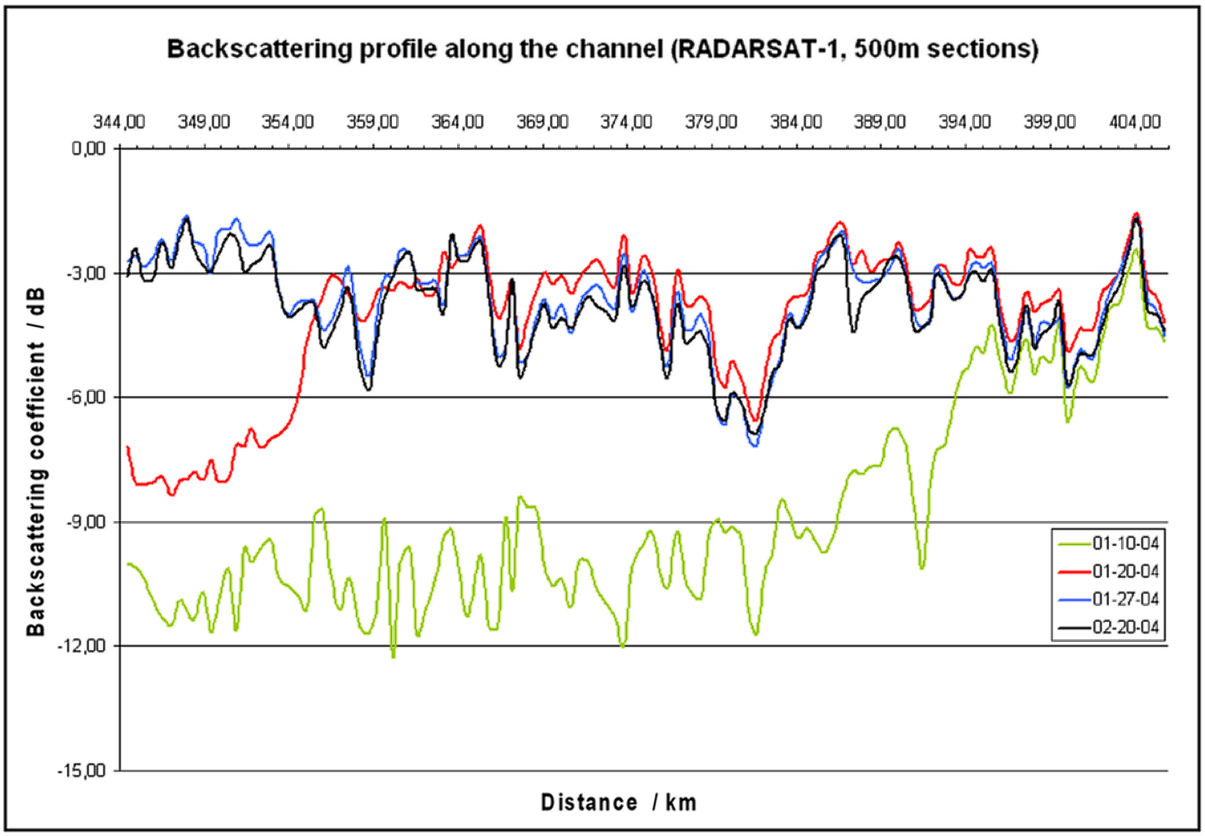

Figure 3: RADARSAT-1 backscattering profile along the river channel (500 m sections, approximately 2,000 to 4,000 pixels each, depending on channel width). The river flows from left to right.

According to the aerial survey, the ice front had progressed upstream to kilometre 356 on January 20. The head of the complete ice cover can be clearly detected at km 356 on the backscattering profile. Again, it is located at the first pronounced peak above -6dB. For both dates, the shift from an incomplete to a complete ice cover is about 4 dB.

On January 27 and February 20, the imaged channel is completely covered by ice. After consolidation, the backscattering profile remains relatively stable over time, which confirms previous observations (5,6). The mean difference is about 5% (0.17 dB). The texture also remains unchanged with an average variation of only 1.3%.

The difference in the backscatter signal for consolidated ice between January 10 and February 20 is small, but is believed to be related to the incidence angle of the images. For example, between km 396 and 406, the lowest backscatter corresponds to the F4 image, which has the largest incidence angle of the four images analysed. Low signal return from an F4 image is to be expected because the backscatter is lower in the far range than in the near range. By way of contrast, the

highest backscatter values are those of the F1N image, which has the lowest incidence angle. The backscatter values of the two F2F images are in between.

ENVISAT ASAR HH images were also compared with RADARSAT-1 images in order to determine whether ASAR data could be used to increase temporal SAR coverage of the river. The river reach that was imaged consists of a consolidated ice cover. Due to slightly steeper incidence angles (Table 1), ASAR images would theoretically be expected to show slightly higher backscattering coefficients than RADARSAT-1 images. However, the opposite was found in this study. As shown in Figure 4, the mean difference is 15% (-0.49 dB) with RADARSAT-1 backscatter coefficients being the larger ones for the February 20 pair. It is 11% (-0.33 dB) for the Jan 27/Feb 1 pair (not shown). In a previous RADARSAT-1 / ASAR comparative study (9), the authors also observed lower ASAR backscatters, but the phenomenon is still under investigation.

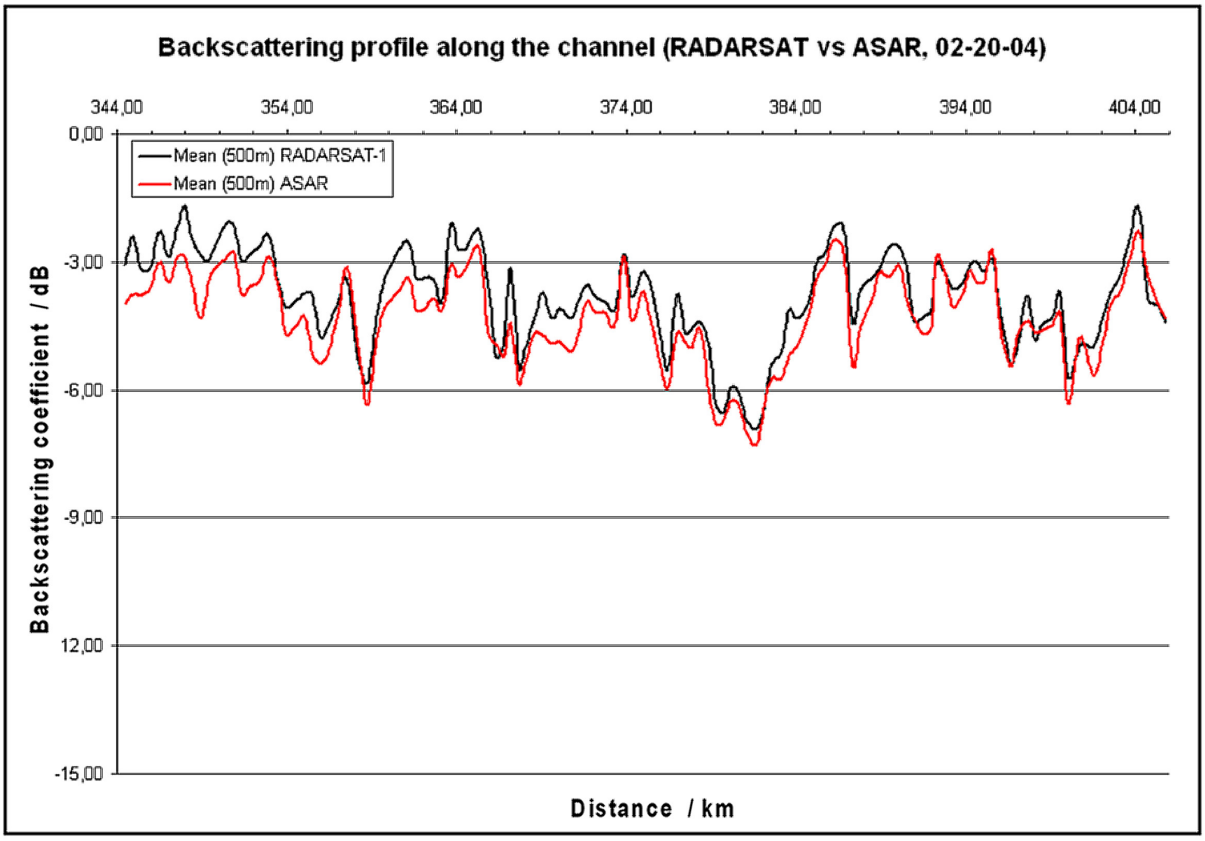

Figure 4: A comparison of RADARSAT-1 and ASAR backscattering profiles along the river channel (500 m sections, approximately 2,000 to 4,000 pixels each for RADARSAT and 500 to 1,000 pixels each for ASAR) on February 20. The river flows from left to right.

Texture profiles of the Peace River study area were compared for the same image pairs discussed above. In both cases, ASAR image texture profiles were 12% greater than RADARSAT-1. The coefficients of determination (R^2) were over 0.83. It was therefore concluded that despite different instruments and spatial resolution, the differences in the ASAR-HH and RADARSAT-1 backscatter values are relatively small to moderate, while the pattern of the backscatter profiles from ASAR-HH and RADARSAT-1 images is similar. Considering the VV polarization, we observe that backscatter from HH and VV polarized ASAR images are not significantly different, as shown with the example of the February 1 profiles (Figure 5). For the three available ASAR images (Table 1), HH backscattering coefficients are slightly higher than VV, with mean differences of 3.5% or less. The texture profiles show mean differences under 1.5%. Therefore, we should not expect any improvement of the classification with the use of a second polarization.

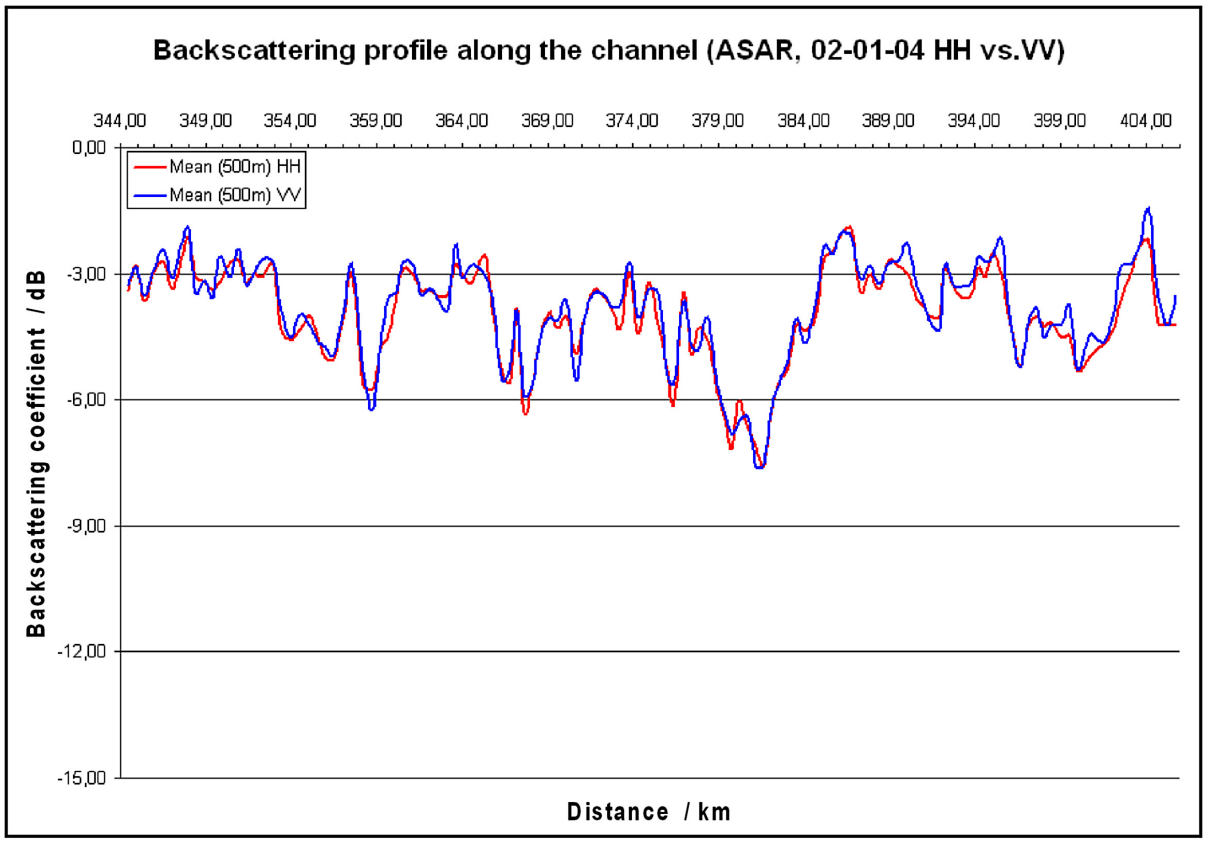

Figure 5: A comparison of ASAR-HH and ASAR-VV backscattering profiles along the river channel (500 m sections, approximately 500 to 1,000 pixels each, depending on channel width) on February 1. The river flows from left to right.

Image classification

The objective of this classification is to accurately map the spatial distribution of ice cover types on the river. The number of classification classes was set to match the number of surface cover types which are visually detectable on the river. This is not an easy task, as the definition of what exactly constitutes a particular ice cover type is somewhat arbitrary at this stage. The boundaries between the individual ice cover types can be vague. Therefore, validating the ice cover classification of the satellite imagery proves difficult and remains subjective.

The number of classes was initially set to seven, which corresponds to the range from smooth water with minimal backscatter to heavily consolidated ice with maximum backscatter. The surface cover types to be expected on the Peace River during the freeze-up period are the following:

- Open water
- Frazil pans (low and high concentrations)
- Freeze over border ice
- Juxtaposed ice
- Consolidated ice (light and heavy degree of consolidation).

Figure 6 shows frazil pans, juxtaposed ice, and consolidated ice.

As explained above, one classification approach only uses backscattering coefficients, while the alternative approach only uses texture values. Based on the respective histograms, classification results are shown in Figure 7 and Figure 8.

Figure 6: Ice types, from left to right: Frazil pans (moderate concentration), juxtaposed ice, consolidated ice.

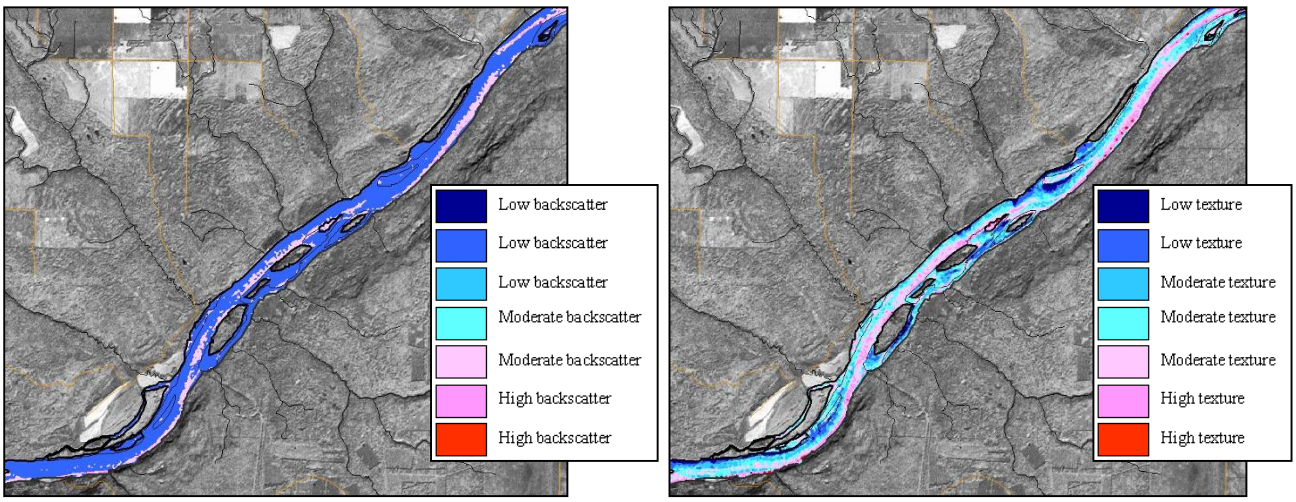

Figure 7: Results from both classification approaches for a section upstream from the ice front (km340-357) – RADARSAT image - January 10, 2004. The river flows from the bottom left to the top right. We consider -10 dB (on a global range of -40 to 0 dB) as a moderate backscatter and 150 (on a global range of 0-255) as a moderate texture.

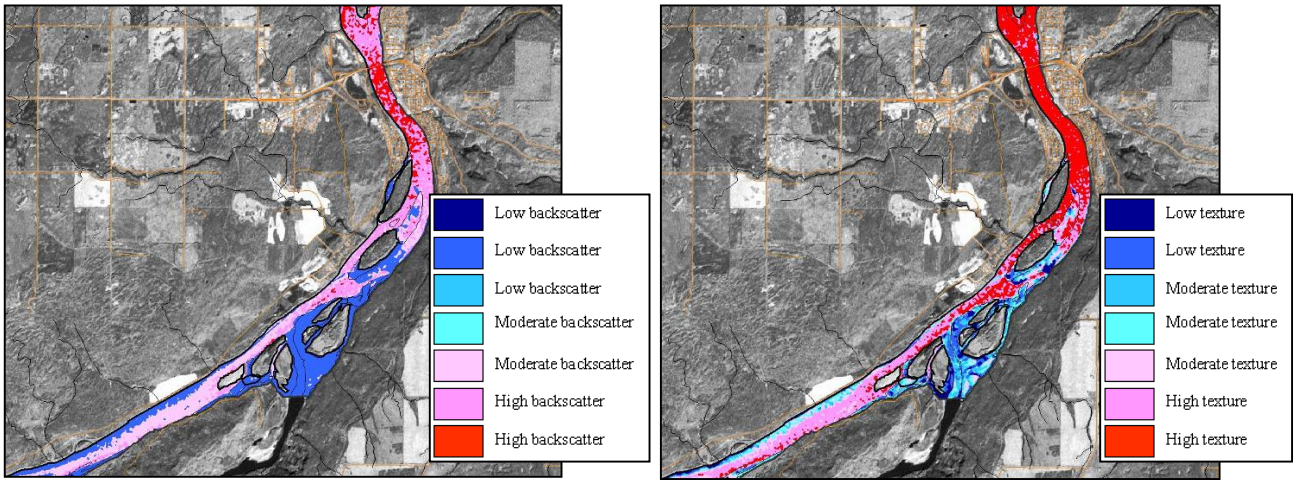

Figure 8: Results from backscatter- (left) and texture-based (right) classifications for a section near the ice front (km382-398) – RADARSAT image - January 10, 2004. The river flows from the bottom left to the top centre. We consider -10 dB (on a global range of -40 to 0 dB) as a moderate backscatter and 150 (on a global range of 0-255) as a moderate texture.

It can be seen that the texture-based classification is efficient in discriminating ice cover types associated with low texture, such as water, border ice, and frazil pans. By comparison, the backscatter-based classification is more efficient in discriminating ice cover types associated with high backscatter, such as juxtaposed and consolidated ice. The difference in sensitivity between both methods is related to the unsupervised nature of the fuzzy K-means classification algorithm and to

the asymmetrical distribution of data fed into the classification (Figure 9). The histogram of the backscattering power values is skewed toward the low values, resulting in more discrimination within the higher classes. By way of contrast, the histogram of texture is skewed toward the high values, resulting in more discrimination within the lower classes.

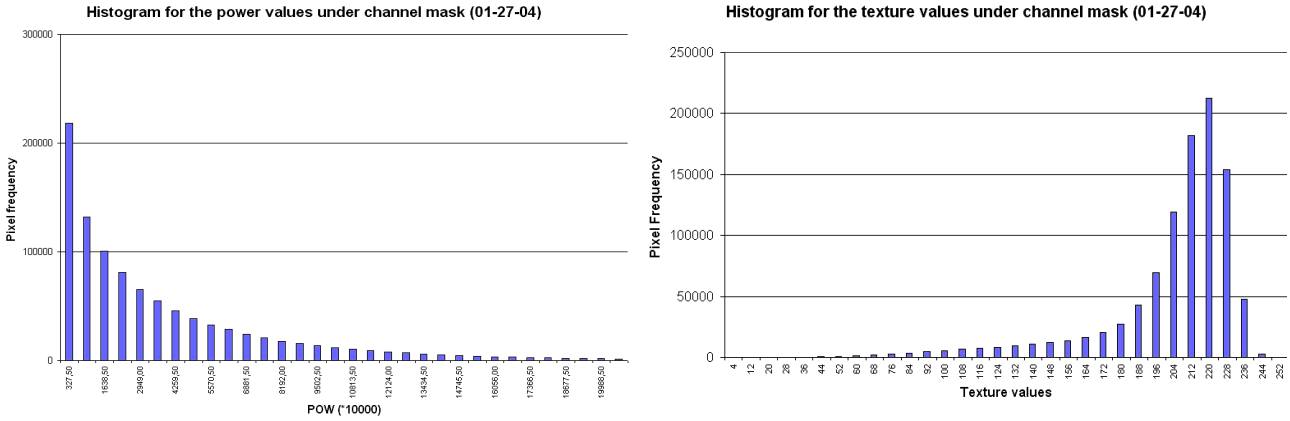

Figure 9: Histograms of power and texture images for January 27, 2004

To achieve the best classification results for the entire range of ice cover types, we propose a four step procedure which combines the two approaches:

1) Apply the texture-based classification to create seven classes
2) Create a mask over the resulting 7th class
3) Apply the backscatter-based classification under this mask only and create two new classes
4) Combine the texture-based classes 1 to 6 and the backscatter-based classes 7 and 8.

As a result, good discrimination is achieved in low backscattering areas (blue classes in Figure 10) as well as in heavily consolidated ice areas (white class in Figure 10). This procedure provided encouraging results for the ice conditions imaged, but more rigorous testing is required for a wider range of ice conditions.

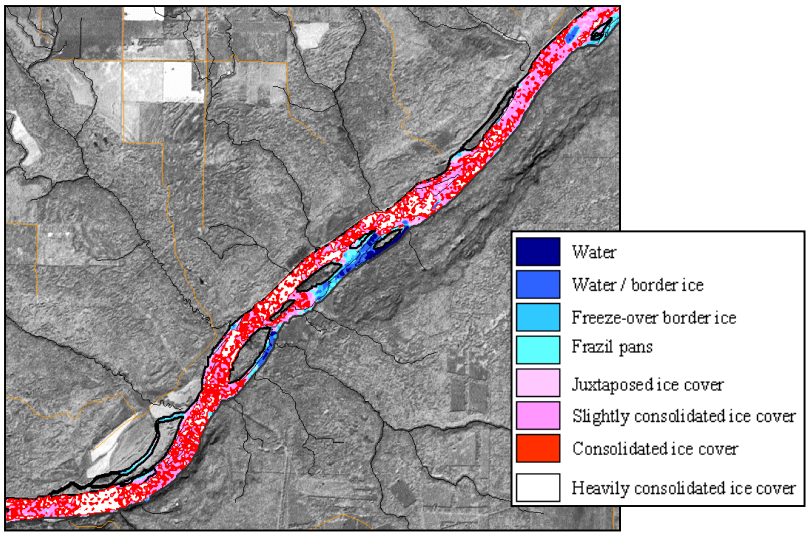

Figure 10: Results of combined classification for a section under consolidated ice (km 340-357), RADARSAT image, February 20, 2004. The river flows from the bottom left to the top right.

The ice cover classifications of the images acquired on February 20, 2004 were visually verified with photographs taken during the aerial survey on the same day. Several sites were chosen for the comparison, like the large ice toe near the Fairview water intake, which formed on January 30 after a consolidation event (Figure 11). The ice ran for 76 km and produced walls 6 m high above the water level. The total ice thickness reached 11 m. The insert in Figure 11 displays the com-

bined ice classification, while class #8 was superimposed onto the georeferenced aerial photo. It can be seen that areas of heavy consolidation match class #8 well. Some areas were still misclassified into class #7. This is probably due to incorrect histogram segmentation by the classifier, inaccuracies in the georeferencing process, and pixel resolution. It should also be noted that the smooth ice in the backchannel (top left of the aerial photo) is clearly mapped in the classification (blue classes).

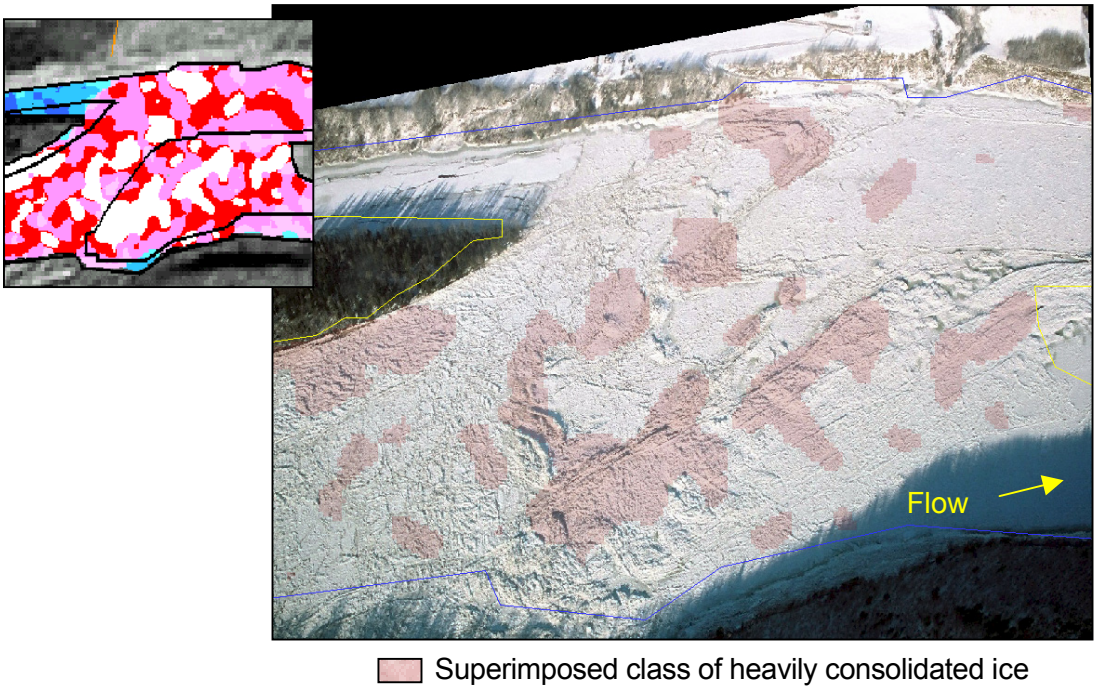

Figure 11: Photo of an area of major ice consolidation, with a translucide superimposition of the white class 8 (heavily consolidated ice) from the combined classification.

Figure 12 shows another comparison between an aerial photograph and an image classification. Open water is generally detected, but inhomogeneous pixels are misclassified. For example, pixels surrounding the open water lead on the left side of the photograph indicate freeze-over border ice, where the map classifies ice cover types typically associated with frazil pans and water/border ice. The size of the open water lead on the right side of the photograph is in the order of the image resolution. The mean texture image averages the pixels of open water and neighbouring ice cover, thereby creating a texture comparable to that typically observed with frazil pans.

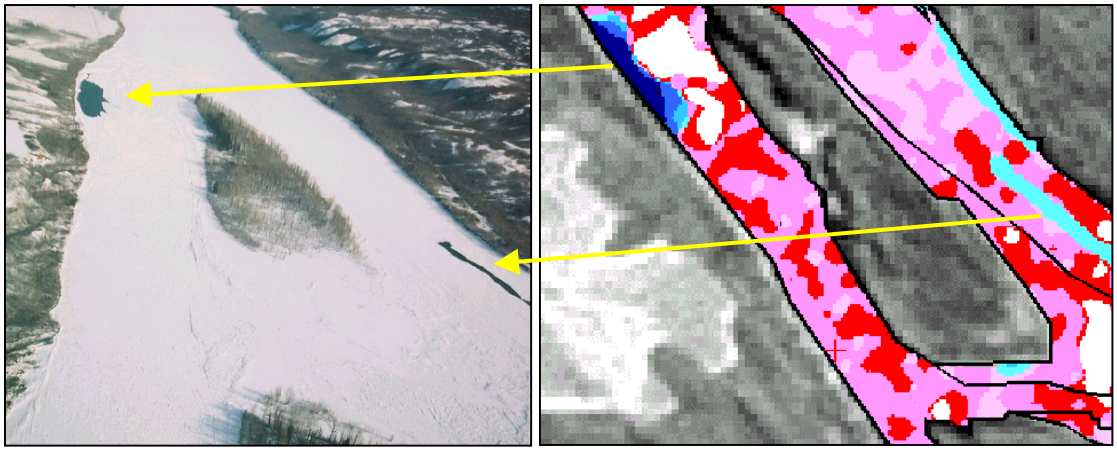

Figure 12: Classification of water areas. The classification is not applied over the islands. Note that on the photo, only the forested part of the island is visible. The other part is masked by snow, as is the surrounding ice cover.

Figure 13 shows the results of the combined classification method when applied to ASAR HH data. Horizontally polarized data produced an ice classification map similar to that derived from RADARSAT-1. Due to ASAR's relatively low resolution, details, such as open water leads, were missed in some instances. For the same reason misclassification arises from pixels which contain several ice cover types, such as open water and juxtaposed ice and consolidated ice. In conclusion, ASAR data reasonably well capture the spatial distribution of the main ice cover types. Its advantage over RADARSAT-1 is lower cost. It was also tested whether adding vertically polarized data as a second input channel would add skill to the classification process. The resulting map (not shown) was of lesser visual quality, because the two channels are highly correlated and, hence, produce speckle.

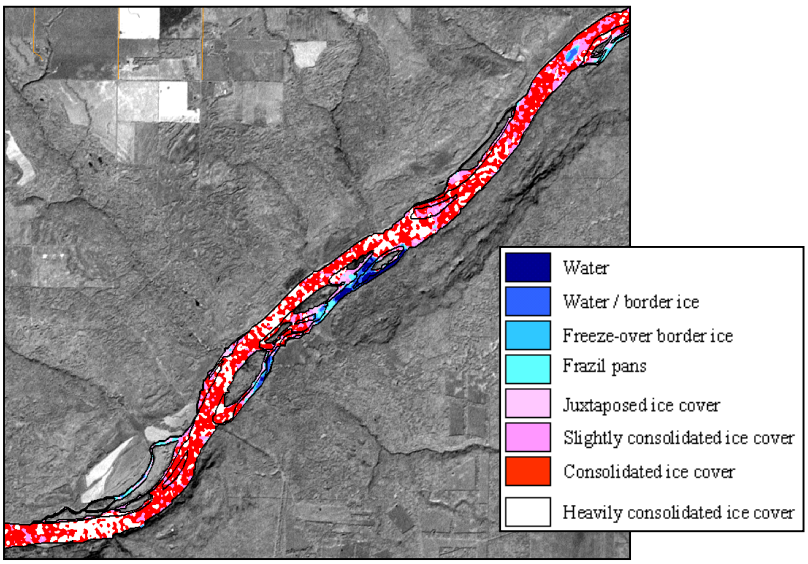

Figure 13: ASAR-HH data classification.

CONCLUSIONS

This project built on several previous river ice studies by the partners involved as well as other agencies. The classification of ice cover types is possible with a relatively high degree of confidence. It was demonstrated that a combination of texture analysis and traditional filtering methods improves the delineation of low backscattering ice cover types without compromising the delineation of high backscattering ice cover types. Ice cover type maps were created which clearly showed the location of the head of the complete ice cover and the spatial distribution of ice cover types upstream and downstream of the head of the complete ice cover. The head of the complete ice cover could also be located on backscatter profiles of the river. The ice cover maps could be used operationally to determine, for example, the head of the complete ice cover, the intensity of frazil ice production, and monitor consolidation events. The ice cover maps are highly self-explanatory and require minimal river ice specific knowledge for interpretation. However, misclassification of ice cover types still occurs. The classification process being unsupervised, we have to be careful in the labelling of the different classes, particularly in the low backscattering / low texture categories, which are more ambiguous. More work is needed to clearly identify these classes. Furthermore, since the procedures were developed for images acquired during freeze-up, they should also be tested during the break-up period.

RADARSAT-1 and ASAR data showed comparable backscattering profiles for 500 m averaged river reaches and produced comparable ice cover maps. In comparison with RADARSAT-1 fine beam images, the relatively coarse resolution of the ASAR data further reduces the sensitivity of the classification by missing details and incorrectly classifying mixed pixels. The addition of the vertical polarization did not improve classification results. Nonetheless, the findings suggest that for a better monitoring of the river ice cover, SAR temporal coverage of the study area can be increased using both RADARSAT-1 and ASAR imagery.

Future work includes the refinement of the classification methodology, the development of a quantitative validation process of the ice map and the development of a theoretical model describing the interaction of radar backscatter and river ice. Many of these aspects are being studied through the international FRAZIL project (Canadian GEOIDE Network funding for 2005-2009).

ACKNOWLEDGEMENTS

This project was financed by GEOIDE (GEomatics for Informed Decisions), as a Strategic Investment Initiative. The images were graciously provided by the Canadian Space Agency. Field measurements were diligently obtained by BC Hydro, Alberta Environment and Trillium Consultants, who patiently showed INRS-ETE's personal what river ice really looked like. We thank all partners.

REFERENCES

1 Page D F & R O Ramseier, 1975. Application of radar technique to ice and snow studies. Journal of Glaciology, 15(73): 171-191

2 Hall D K, D B Fagre, G Linebaugh & G E Liston, 1994. Analysis of ERS-1 synthetic aperture radar data of frozen lakes in northern Montana and implication for climate studies. Journal of Geophysical Research, 99(C11) 22: 473-482

3 Jefferies M O, K Morris & W F Weeks, 1994. Structural and stratigraphic features and ERS-1 synthetic aperture radar backscatter characteristics of ice growing on shallow lakes in NW Alaska, winter 1991-1992. Journal of Geophysical Research, 99(C11) 22: 459-471

4 Leconte R & P D Klassen, 1991. Lake and river ice investigations in Northern Manitoba using airborne SAR imagery. ARCTIC, 44(1): 153-163

5 Weber F, D Nixon & J Hurley, 2003. Semi-automated classification of river ice types on the Peace River using RADRASAT-1 Synthetic Aperture Radar (SAR) imagery. Canadian Journal of Civil Engineering, 30: 11-27

6 Jasek M, F Weber & J Hurley, 2003. Ice thickness and roughness analysis on the Peace River using RADARSAT-1 SAR imagery. In: 12th Workshop on the Hydraulics of Ice Covered Rivers (CRIPE), (Edmonton, Canada) 50-68 (Published on CD-ROM)

7 Hall-Beyer M, 2005. The GLCM Texture Tutorial, Version 2.8 (University of Calgary, Canada)

8 Tso B & P M Mather, 2001. Classification Methods for Remotely Sensed Data (Taylor and Francis) 332 pp.

9 Gauthier Y, S Hardy, M Bernier & M Carignan, 2005. Comparison of RADARSAT-1 and ASAR data for cryospheric applications in Canada: the case of Snow Water Equivalent. In: Proceedings of the 2004 ENVISAT and ERS Symposium, 6-10 September 2004, Salzburg, Austria. ESA SP-572, April 2005 (ESA Publications Division, ESTEC, Noordwijk, The Netherlands)